CSCE Annual Conference

Growing with youth – Croître avec les jeunes

Laval (Greater Montreal)

June 12 - 15, 2019

Evaluation of the Bond-Dependent Coefficient for Ribbed-Deformed GFRP Bars in Concrete Beams

Shang, C.[1,3], Mahmoud, K.[2,4], Bediwy, A[1,5], El-Salakawy, E.[1,6]

[1] University of Manitoba, Canada
[2] Assuit University, Assiut, Egypt
[3] shangc@myumanitoba.ca
[4] karam.awad2005@gmail.com
[5] bediwya@myumanitoba.ca
[6] Ehab.El-Salakawy@umanitoba.ca

Abstract: In this paper, test results of four glass fiber-reinforced polymer (GFRP)-reinforced concrete simply supported beams are presented. This experimental study aims at evaluating the bond-dependent coefficient (k_b) and verifying its dependency on bar diameter and concrete cover in normal-strength concrete beams. Only deformed/ribbed GFRP bars were used as main longitudinal reinforcement in all beams. The beam specimens were 2,800 mm long × 200 mm wide × 300 mm deep and were tested in flexure under four-point bending configuration over a simply supported span of 2,400 mm with 200 mm overhang on each side. The test results showed that the bar diameter and concrete cover affected the crack width and consequently the value of k_b. Also, the average k_b was found to be 0.9 for ribbed GFRP bars which is lower than the current recommendations in codes and guidelines for deformed/ribbed FRP bars.

1 INTRODUCTION

Fiber-reinforced polymer (FRP) bars are being used as reinforcement in concrete structures such as overpasses, bridges and parking garages in which the corrosion of conventional steel reinforcement has typically led to significant deterioration and rehabilitation needs. Due to the rapid development of the FRP industry, new glass FRP (GFRP) products with different surface treatment and mechanical properties are currently in the market including indented, helically-grooved, deformed/ribbed, and sand-coated. There is a need for research utilizing these new products to validate/improve the accuracy of design codes and guidelines for the design and construction of FRP-reinforced concrete (RC) structures. However, the design codes and guidelines (CSA/S806-12 2017 and ACI 440.1R-15 2015) provide specific values for the bond-dependent coefficient (k_b) only according to surface characteristics of the FRP bars and neglecting concrete cover and bar diameter as well as type of transverse reinforcement. Providing more accurate k_b value will lead to a significantly reduced amount of FRP reinforcements since, in most cases, the crack width governs the design of GFRP-RC structures.

This study aims at evaluating the k_b for deformed/ribbed GFRP bars with different bar diameter and concrete cover experimentally in normal-strength concrete beams. Also, the value of the experimentally obtained k_b is compared to that in the current codes and guidelines for FRP-RC structures.

2 EXPERIMENTAL PROGRAM

2.1 Material Properties

Reinforcing Bars: Size No. 10M grade 400 deformed steel bars were used as top longitudinal reinforcement and stirrups, where applicable, in this study. The mechanical properties of the conventional steel reinforcing bars (Table 1) were obtained through tensile tests carried out in the laboratory according to CSA/G30.18-09 (CSA 2009). On the other hand, the main longitudinal reinforcement was deformed/ribbed GFRP bars, size No. 16 and No.19, as shown in Fig. 1(a). The characteristic design values such as strength and strain of GFRP bars, defined by CSA/S806-12 (CSA 2017), were based on the material certificate provided by the manufacturer (Table 3.3). In addition, size No.13 sand-coated GFRP bent bars was used as transverse reinforcement in one specimen. Figure 1(b) shows photos of the two types of the stirrups. Table 1 summarizes the mechanical properties of the reinforcing bars.

Table 1: Tensile properties of the reinforcing bars

Bar material	Bar size	Nominal diameter (mm)	Nominal area (mm^2)	Tensile strength (MPa)	Elastic modulus (GPa)	Ultimate strain (%)
Steel	10M	11.3	100	400[a]	200	0.21[a]
Sand-coated GFRP (Bent)	No.13	12.7	127	1,280[b]	52[b]	2.5[b]
Ribbed-Deformed GFRP (Straight)	No.16	16	200	1,100	60	1.83
	No.19	20	314	1,060	64	1.67

[a] yield stress and strain for steel
[b] Straight portion property
Note: The properties of the GFRP bars are calculated based on the nominal area.

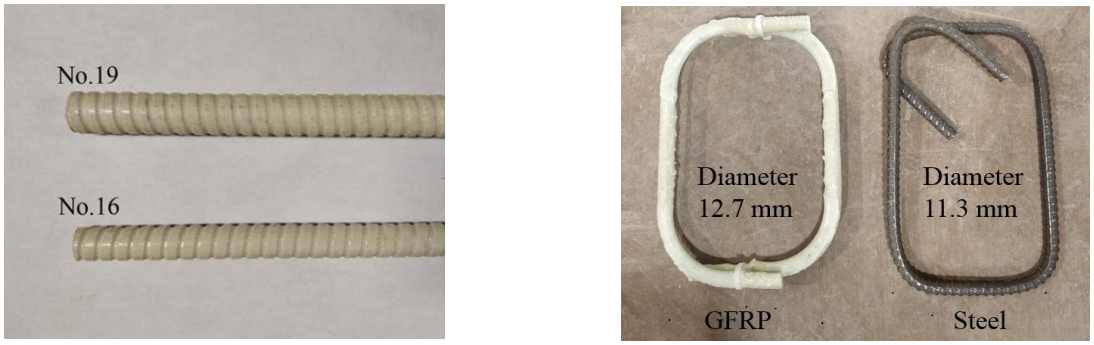

(a) Ribbed/deformed straight bars (b) stirrups

Figure 1: Beam reinforcement

Concrete: The concrete beams were constructed using normal-weight ready-mix concrete with a target 28-day compressive strength of 35 MPa. The maximum size of the coarse aggregates was 20 mm. The concrete compressive strength of each batch was determined by testing five 100 × 200 mm cylinders while the tensile strength was determined by split-cylinder test using five 150 × 300 mm cylinders. Table 2 provides the concrete compressive and tensile strengths.

2.2 Test Specimens

A total of four large-size simply supported rectangular beams reinforced with deformed/ribbed GFRP bars were constructed and tested to failure. The test beams were 2,800 mm long × 200 mm wide × 300 mm deep. The beams were reinforced with one layer of two GFRP bars as bottom reinforcement. The top

reinforcement for all beams consisted of two 10M steel bars. To minimize the confining effect of the shear reinforcement on the flexure behaviour, no stirrups were used in the constant moment zone. The test parameters of this experimental program were bar diameter (16 and 19 mm) and concrete cover (38 and 50 mm). In three beams, steel stirrups were used as transverse reinforcement while in the fourth beam a GFRP stirrups were used. The nomenclature of the test beams can be explained as follows: R for ribbed-deformed bars; then bar diameter (16 and 19 mm); C stands for the concrete cover used in the specimens (38 and 50 mm); finally, the type of transverse reinforcement (I for steel stirrups and II for GFRP bent bars). Figure 2 and Table 2 provide the specimens dimensions and reinforcement details.

2.3 Instrumentation and Test Setup and procedure

The beams were tested under four-point bending over a clear span of 2,400 mm. The beams had a clear shear span of 900 mm and 38/50 mm clear concrete cover, while the distance between the two loading points was 600 mm. Four electrical strain gauges were glued on the bottom GFRP longitudinal bars at the middle of the beam and at loading points (Fig. 2). In addition, one strain gauge was installed on the top surface of the concrete beam to measure the compressive strains in the concrete at the mid-span section. The mid-span deflection for the tested beams was monitored using a linear variable displacement transducer (LVDT) and another LVDT was used to measure the first flexural crack width in the constant moment zone of test beams. In addition, three 200-mm PI gauges were installed on the beam's side surface of the constant moment zone (at the reinforcement level) to account for the total elongation induced by flexural cracks. Table 2 shows the details of test beams.

A hydraulic testing machine was used to apply the two equal concentrated loads on the beam specimens through a spreader beam at a stroke-controlled rate of 1.2 mm/min. The loading was paused when the first flexural cracks appeared, and the initial crack widths were measured manually using a handheld microscope. Thereafter, a high accuracy LVDT was installed to continuously monitor the crack width with the load increase. Figure 3 shows a photo of one beam in the setup ready for testing.

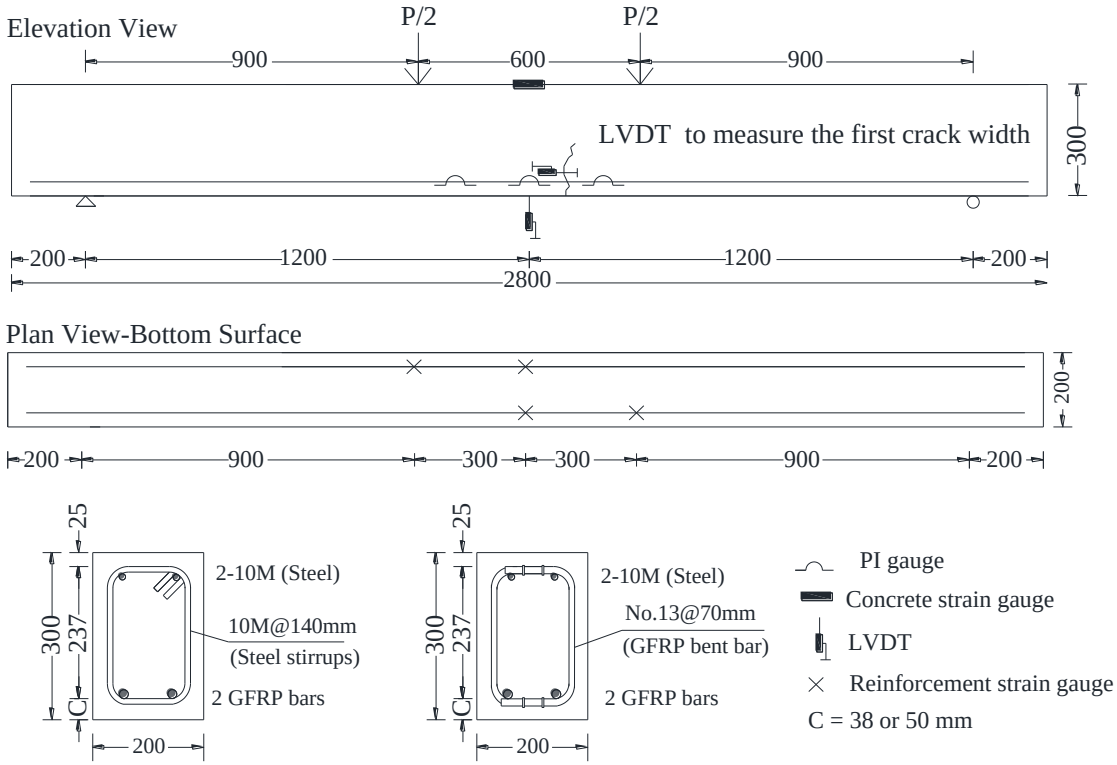

Figure 2: Typical location of instrumentation and test setup

Table 2: Properties and reinforcement details of the test beams

Beam	Compressive strength, f_c', (MPa)	Tensile strength, f_t, (MPa)	Concrete cover (mm)	Longitudinal reinforcement				Transverse reinforcement	
				Bars	ρ_f (%)	ρ_f/ρ_{fb}	$E_f A_f$ (kN)	Bar size	Spacing (mm)
R16-C38-I	44	4.0	38	2-No.16	0.65	1.79	24,000	No.10M	140
R16-C50-I	44	4.0	50	2-No.16	0.69	1.88	24,000	No.10M	140
R19-C50-I	44	4.0	50	2-No.19	1.16	2.86	40,192	No.10M	140
R16-C38-II	41	3.9	38	2-No.16	0.65	1.79	24,000	No.13	70

Figure 3: Overview of the test setup

3 TEST RESULTS AND DISCUSSION

3.1 Cracking Pattern, Cracking Moment and Mode of Failure

The cracking patterns of the test beams at failure are shown in Fig. 4. The first crack appeared in the constant moment region of the test beams, starting from the bottom surface of the beam and extending vertically toward the top compression zone. The cracks were vertical, perpendicular to the direction of the maximum principle tensile stress induced by pure bending. The first crack in the constant flexural moment zone was visually observed at a load of 19.4, 21.0, 20.6 and 22.7 kN in beams R16-C38-I, R16-C50-I, R19-C50-I and R16-C38-II, respectively. These loads correspond to approximately 11, 13, 10 and 14% of the failure load of the beams, respectively. With increasing the load, additional flexural cracks appeared, which reduced the crack spacing. Cracks outside the constant-moment region formed at approximately 20% of the ultimate load and affected by a combination of flexural and shear stresses. Finally, the failure in all test beams took place due to crushing of concrete (compression failure). As expected, the beams with higher reinforcement ratios, experienced more tensile cracks of smaller width extending away from the constant moment region towards the supports.

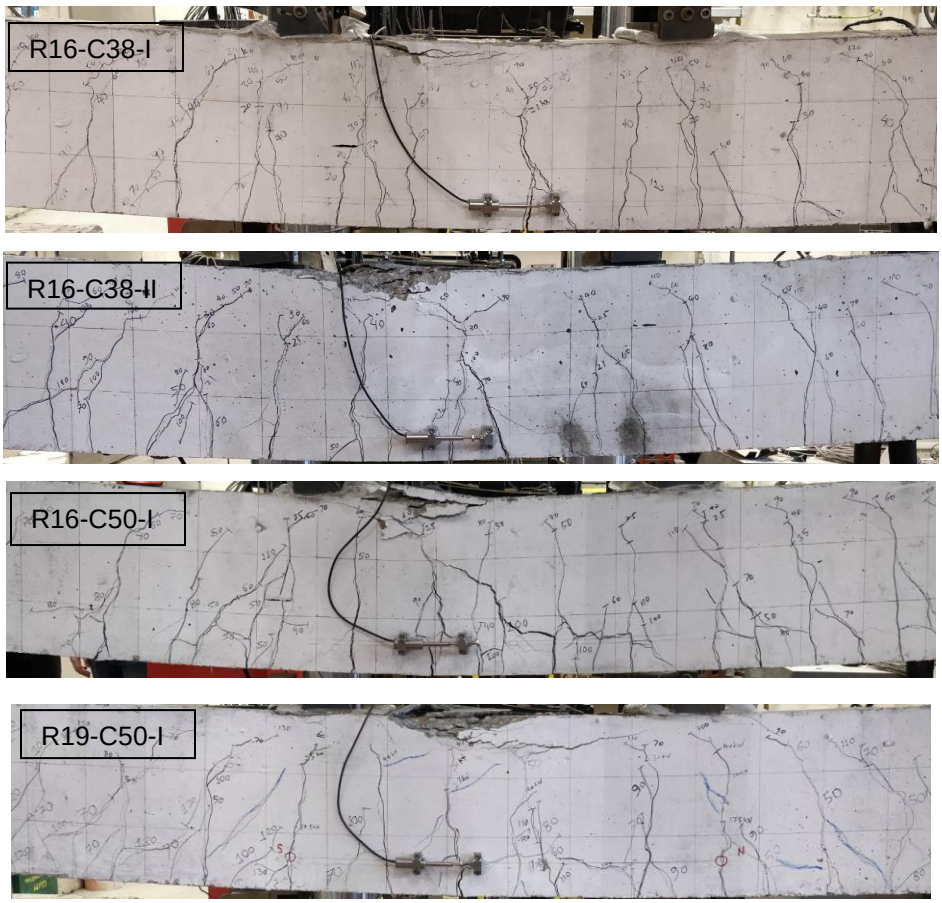

Figure 4: Cracking patterns in the constant moment region of test beams at failure

Table 3 lists the experimental and predicted values of the cracking moments. The cracking moments (M_{cr}) were calculated using Equation (1) where f_r is the modulus of rupture of concrete and is calculated from Equations (2) and (3) in accordance with CSA/S806-12 (2017) and ACI 440.1R (2015), respectively, for normal-density concrete ($\lambda = 1$).

The cracking moment of the GFRP-RC beams was generally 20% and 22% lower than those predicted by CSA/S806-12 (CSA 2017) and ACI 440.1R (2015), respectively.

[1] $M_{cr} = \frac{f_r \times I_g}{y_t}$

[2] $f_r = 0.60\lambda\sqrt{f_c'}$

[3] $f_r = 0.62\lambda\sqrt{f_c'}$

Based on Table 3, the CSA/S806-12 (2017) yielded slightly better predictions of cracking moments than ACI 440.1R (2015) due to the smaller modulus of rupture values. Similar observations were reported for the cracking moments of GFRP-RC beams (El-Nemr et al. 2013) where the predicted cracking moments were higher than the measured ones.

Table 3: Experimental and predicted values of the cracking moments

Beam ID	Experimental M_{cr} (kN.m)	MOF[a]	CSA/S806 (2017) $\frac{M_{cr,Exp.}}{M_{cr,pre.}}$	ACI 440.1R (2015) $\frac{M_{cr,Exp.}}{M_{cr,pre.}}$
R16-C38-I	8.8	CC	0.74	0.71
R16-C50-I	9.5	CC	0.8	0.77
R19-C50-I	9.3	CC	0.78	0.76
R16-C38-II	10.2	CC	0.89	0.86
Average			0.80	0.78
Standard deviation			0.05	0.05

[a] CC: crushing of concrete

3.2 Deflection Behaviour

Figure 5 shows the moment versus the mid-span deflection relationship for the test beams. The test GFRP-RC beams demonstrated typical bi-linear moment-deflection relationship. All the beams had nearly similar pre-cracking stiffness and cracking loads which is due to the negligible effect of the reinforcement ratio on the gross moment of inertia of the beam section. In the post-cracking stage, all tested beams exhibited lower post-cracking stiffness until failure. When the applied moment exceeded the cracking moment, the cracking occurred in the mid-span (constant-moment region), causing a reduction in stiffness and drop in slope of the moment-deflection curve. It was observed that the axial stiffness and reinforcement ratio had a significant influence on the beams post-cracking response until failure. As expected, the higher the reinforcement ratio, the higher the post-cracking stiffness and, consequently, the lower the deflection values. In addition, it was also observed that the thickness of concrete cover affected the beam post-cracking deflection response. Beams R16-C38-I and R16-C38-II, with similar axial stiffness of 24,000 kN, had slightly steeper load-deflection curves than that of beam R16-C50-I. This is due to the larger beam depth associated with smaller concrete cover (38 mm) which resulted in a relatively larger flexural stiffness (EI_e) after cracking compared to the beam with larger concrete cover (50 mm). Moreover, the load-deflection relationships were not affected by the type of transverse reinforcement when the same axial stiffness was provided.

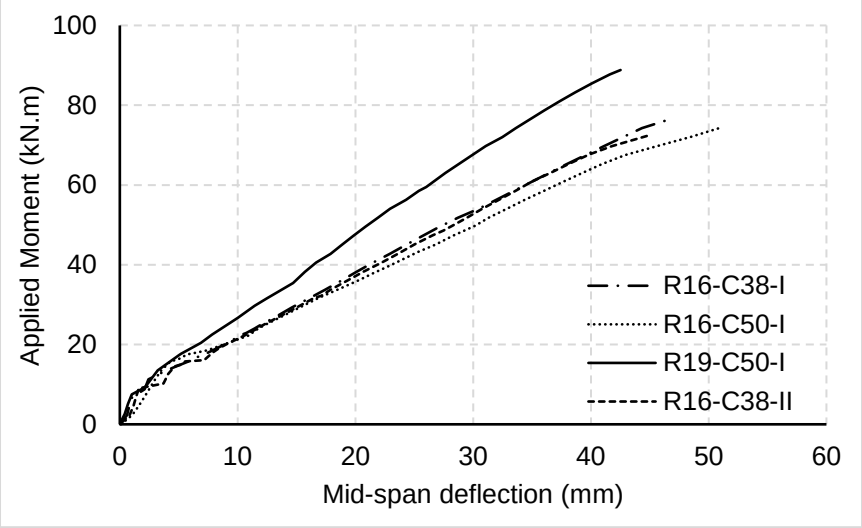

Figure 5: Moment-deflection relationship at mid-span of test beams.

3.3 Crack width

Figure 6 shows the moment-versus-crack width relationship for the tested beams at mid-span. The service load was calculated as recommended in different codes and guidelines at 2,000 micro-strains, 0.3M_n and 0.25f_{frpu} for all beams. It was observed that beam with the highest reinforcement ratio and axial stiffness, R19-C50-I showed the smallest crack width at the same load level compared to beam R16-C50-I. Also, the thickness of concrete cover influenced the crack width of the test beams at the service-load level. In beams reinforced with No.16 deformed/ribbed GFRP bars, R16-C38-I showed relatively larger crack width value at service load compared to that of R16-C50-I (0.42, 0.67 and 0.69 mm compared to 0.40, 0.55 and 0.57 mm, respectively). This confirms that the bond-dependent coefficient (k_b) value considering only bar surface configuration (regardless of concrete cover) is not accurate and does not reflect the actual behaviour. Moreover, at the load level at which the strain in the longitudinal reinforcement reached 2,000 micro-strains, all beams satisfied the service-limiting flexural crack width of 0.5 mm specified by CSA/S6 (2014) and CSA/S806 (2017).

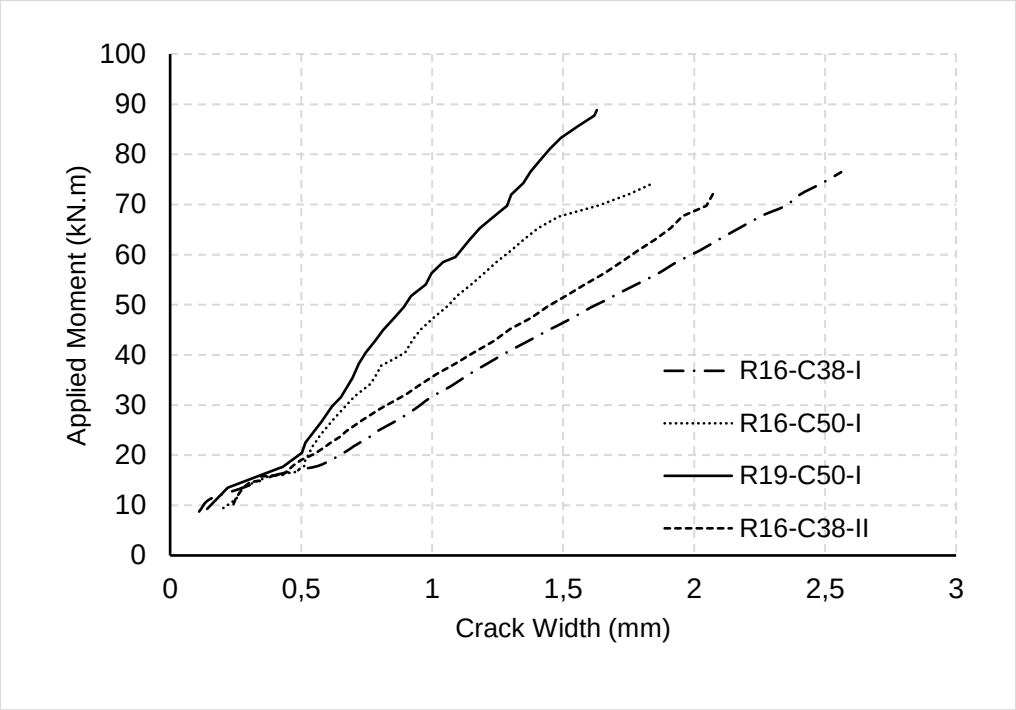

Figure 6: moment-versus-crack width for the test beams at mid-span region

3.4 Bond-Dependent Coefficient (k_b) Prediction

Table 4 shows the average k_b values at different limits calculated from Eq. (4) and (5) according to ACI 440.1 R-06 (ACI Committee 440 2006), ISIS Manual No.3 (2007) and CSA/S6-14 (CSA 2014). It is worth mentioning that the average k_b values determined at the suggested service load which is corresponding to crack width (w) = 0.7 mm, a moment of 0.30M_n, and a stress in the longitudinal reinforcement of 0.25f_{frpu}.

[4] $w = \frac{2.2}{E_f}\gamma k_b f_f \sqrt[3]{d_c A}$

[5] $w = 2\frac{f_f}{E_f}\beta k_b \sqrt{{d_c}^2 + (s/2)^2}$

For the deformed/ribbed GFRP bars, the average k_b values determined according to ACI 440.1 R-06 (ACI Committee 440 2006) and the CSA/S6-14 (CSA 2014) were 1.1, 0.7, 0.8, and 1.1 for R16-C38-I, R16-C50-I, R19-C50-I and R16-C38-II, respectively, with an average of 0.9. ISIS Manual No.3 (2007) equation yielded k_b values of 0.8, 0.5, 0.5, and 0.7 for R16-C38-I, R16-C50-I, R19-C50-I and R19-C38-II, respectively, with an average of 0.6. The result indicated the measured k_b values were smaller than the recommended k_b values according to ACI 440.1 R-06 (ACI Committee 440 2006) and the CSA/S6-14 (CSA 2014), ISIS Manual No.3 (2007).

The results reported in Table 4 also indicate the effect of concrete cover on the calculated k_b values. For beams with No.16 deformed/ribbed GFRP bars, when the concrete cover increased from 38 mm in beam R16-C38-I to 50 mm in beam R16-C50-I, the average k_b value decreased 1.1 to 0.7.

In addition, it can be observed that the bar diameter had a significant effect on k_b value. For beams R16-C50-I and R19-C50-I, with the same thickness of concrete cover, when the bar diameter increased from 16 mm to 19 mm the average k_b value increased from 0.7 to 0.8, respectively. This might be due to the tendency for GFRP bars of larger diameter to show lower bond to the surrounding concrete.

Table 4: Average predicted k_b values in comparison with the design recommendations

Beam ID	k_b average ACI 440.1 R-06 (2006); CSA/S6-14 (2014)	k_b average ISIS Manual No.3 (2007)	ACI 440.1 R-06 (2006)	ISIS Manual No.3 (2007)	CSA/S6-14 (2014)
R16-C38-I	1.1	0.8	1.4 (excluding smooth bars and grids)	1.2 (In the absence of significant test data)	0.8 (Sand-coated FRP)
R16-C50-I	0.7	0.5			
R19-C50-I	0.8	0.5			
R16-C38-II	1.1	0.7			

4 CONCLUSIONS

Based on test results and discussions presented herein, the following conclusions were drawn:

1- As the bar dimeter increased from 16 to 19 mm, the crack width decreased as a result of the higher axial stiffness of the reinforcement. Also, beam with larger concrete cover (50 mm) had a smaller crack width compared to that of beam with smaller concrete cover (38 mm) at service load level.
2- Increasing the concrete cover from 38 to 50 mm caused a decrease in the average k_b value for No.16 deformed/ribbed bars from 1.1 to 0.7, respectively. In addition, increasing the bar diameter while keeping the same thickness of concrete cover caused increase in the k_b values for deformed/ribbed bars from 0.7 to 0.8.
3- The average k_b was 0.9 for ribbed GFRP bars which is lower than the current recommendations for deformed/ribbed FRP bars by the CSA/S6-14 (2014), ACI 440.1 R-06 (2006) and ISIS Manual No.3 (2007).

5 ACKNOWLEDGMENTS

The authors wish to acknowledge the financial support received from the Natural Science and Engineering Research Council (NSERC) of Canada. Also, the help received from the technical staff of McQuade Heavy Structures Laboratory of University of Manitoba is greatly acknowledged.

6 REFERENCES

ACI Committee 440. 2006. “Guide for the Design and Construction of Structural Concrete Reinforced with FRP Bars.” ACI 440.1R-06. *American Concrete Institute*, Detroit, MI, 44 p.

ACI Committee 440. 2015. “Guide for the Design and Construction of Structural Concrete Reinforced with FRP Bars.” ACI 440.1R-15. *American Concrete Institute*, Detroit, MI, 83 p.

Canadian Standard Association (CSA), 2014. Canadian Highway Bridge Design Code (*CAN/CSA S6-14*). Rexdale, ON, Canada.

CSA (Canadian Standards Association). 2009. “Carbon steel bars for concrete reinforcement.” G30.18-09, Rexdale, ON, Canada.

Canadian Standard Association (CSA). 2017. Design and Construction of Building Structures with Fibre Reinforced Polymers, *CAN/CSA S806-12 (R2017)*. Rexdale, ON, Canada

El-Nemr, A., Ahmed, E., and Benmokrane, B. 2013. “Flexural behavior and serviceability of normal- and high-strength concrete beams reinforced with glass fiber-reinforced polymer bars”, *ACI Structural Journal*, 110(6), 1077–1088.

ISIS Manual No 3. 2007. “Reinforcing Concrete Structures with Fibre-Reinforced Polymers.” *ISIS Canada Research Network*, University of Manitoba, Winnipeg, MB.